Radiological Physics and Technology (2019) 12:194–200
https://doi.org/10.1007/s12194-019-00514-w

Image quality parameters in brain imaging with fan-beam collimator: a Monte Carlo study on radiation scattering effects

Hamid Reza Baghani[1]

Received: 28 January 2019 / Revised: 10 April 2019 / Accepted: 10 April 2019 / Published online: 13 April 2019

Abstract
The effects of scattered radiation on image quality in brain imaging with fan-beam collimator were quantitatively evaluated. A commercial gamma camera in conjunction with a fan-beam collimator was simulated using MCNPX code. The effects of radiation scattering on image quality were evaluated by employing the Snyder phantom and comparing the system response to an isotropic ^{99m}Tc point source in both spatial and frequency domains. The trans-axial spatial resolution of the obtained point spread functions were studied in the spatial domain, at source-to-collimator distances of 2, 4, 6, 8, and 10 cm. At the same distances, the spatial frequencies at 90% ($SF_{0.9}$) and 10% ($SF_{0.1}$) of the maximum modulation transfer function were considered in the frequency domain. The maximum difference between the obtained full width at half-maximum in presence and absence of phantom was approximately 5%, while this difference was 14% for full width at tenth maximum. An analysis of system response in the frequency domain demonstrated a large difference of 43% between the obtained $SF_{0.9}$ values in presence and absence of phantom. In contrast, this difference was a mere ~2% between the obtained $SF_{0.1}$ values. Radiation scattering mainly degrades the image contrast resolution and has no considerable effect on the spatial resolution of the images acquired by the fan-beam collimator. Accordingly, the impact of radiation scattering on image quality was more obvious in frequency domain, and $SF_{0.9}$ can be considered as an operational parameter for the quantitative assessment of radiation scattering effects on image quality in the frequency domain.

Keywords Fan-beam collimator · Brain imaging · Image quality · Monte Carlo simulation

1 Introduction

One of the main objectives in nuclear medicine, which more often than not goes hand in hand with clinical practice, is the improvement of lesion diagnosis by tracing the radio-pharmaceutical uptake inside the body. Single-photon emission computed tomography (SPECT) is of the most frequently applied nuclear medicine imaging modalities used to assess the lesion distribution and its function. The procedure involves the injection of a specific gamma emitter into the patient and the detection of the emitted gamma rays from the patient body using a gamma camera [usually a sodium iodide (NaI) scintillation detector] [1].

Compton scattering is one of the main features of radiation interaction with the patient body that unfortunately degrades the quality of the images obtained by this imaging modality. The presence of a collimator is essential for the projection view and image formation, as it inherently reduces the contribution of Compton scattering through absorption of the scattered photons by the collimator body. One of the collimator types employed in SPECT is the fan-beam collimator, which is a combination of a converging/pinhole collimator and a parallel-hole collimator in two different dimensions; this combination can take advantage of both the collimators' features at once [2].

Because of the inherent magnification in this combined collimator type, the contribution of the spatial resolution of the camera to that of the entire system decreases inversely with the collimator magnification coefficient [2]. Resultantly, this combined collimator can be substituted by a parallel-hole collimator in imaging applications that involve the brain or small organs such as the thyroid [3, 4]. Hence, the improved spatial resolution and image quality comprise the main reasons that justify the application of fan-beam collimators in the SPECT imaging technique.

✉ Hamid Reza Baghani
hamidreza.baghani@gmail.com

[1] Physics Department, Hakim Sabzevari University, Shohada-e Hastei Blvd, Sabzevar 9617976487, Iran

The application of fan-beam collimators in nuclear medicine imaging has been studied by several authors [5–10]. However, not much attention has been paid to the effect of scattered radiation on the quality of the image acquired by such collimators. Therefore, the objective of this study was to evaluate the effect of radiation scattering on the quality of brain SPECT images acquired by the fan-beam collimator. To this end, a commercial gamma camera model in conjunction with the fan-beam collimator was simulated using the MCNPX Monte Carlo code and the effects of scattered radiation on image quality were quantitatively evaluated with the point spread function (PSF) and the modulated transfer function (MTF) in both spatial and frequency domains, respectively.

2 Materials and methods

2.1 Monte Carlo modeling of SPECT imaging system

The SPECT imaging system simulated in the current study was the SPECT modality of a Discovery NM-CT 670 hybrid scanner manufactured by the General Electric (GE) Company [11]. Simulations were performed using the Monte Carlo MCNPX code [12], and the physical and geometric characteristics of the simulated gamma camera were provided by the manufacturer. The simulated gamma camera was a sodium iodide scintillation crystal (NaI) with a thickness of 0.375 in. Because the MCNPX code is not able to generate and track the generated photons during the scintillation process inside the crystal, the simulated gamma camera (NaI crystal) was divided into several pixels with defined dimensions to consider the effects of light spreading inside the crystal and the inherent spatial resolution of the gamma camera. As the inherent spatial resolution for most gamma cameras is approximately 4 mm [13, 14], the size of each pixel was set to 4×4 mm^2. Furthermore, the limited energy resolution of the gamma camera can also affect the contribution of scattered photons to the signal acquired by the camera. Therefore, the limited energy resolution of the gamma camera was also considered in the simulation by tuning the energy response of the simulated gamma camera to a Gaussian response, using the Gaussian energy broadening (GEB) option defined in the MCNPX code [12]. The validity of this energy tuning procedure was evaluated by a comparison of the calculated and measured energy response of the gamma camera at an energy input of 140 keV. To this end, an isotropic ^{99m}Tc point source was positioned at a distance of 10 cm from the front surface of the gamma camera, and the pulse height of spectra obtained by the measurement was compared with the Monte Carlo simulated pulse height spectra.

Table 1 Specifications of simulated fan-beam collimator

Collimator type	Hole shape	Hole diameter (mm)	Focal length (mm)	Septal thickness (mm)[a]	Height (mm)
Fan-beam	Hexagonal	1.5	350	0.3	25

[a]Septal thickness is defined at the narrow end of the collimator, i.e., toward the patient

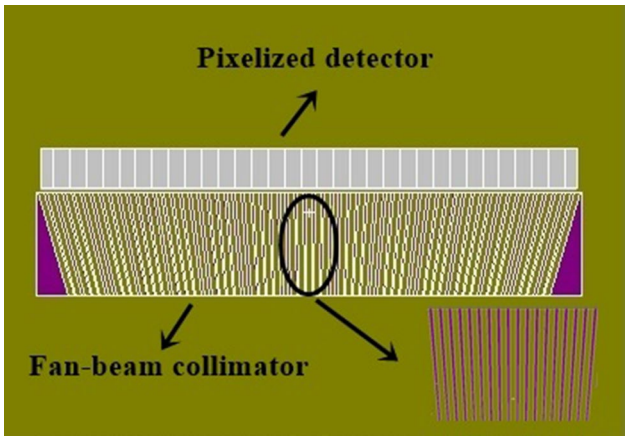

Fig. 1 Simulated gamma camera in conjunction with fan-beam collimator. The gamma camera is considered to be a pixelized detector with an intrinsic spatial resolution, which is included in the simulations. The circle shows an enlarged image of the simulated fan-beam collimator; both the collimator holes and septal thickness are also shown

To perform a detailed modeling for the fan-beam collimator, first, the rotation angle of each collimator hole, with respect to the central one, was calculated by the trigonometric relationships and then the position of each collimator hole was determined by applying the calculated angles to the regular form of the rotation matrix in space. Finally, the obtained geometric data for each hole were considered in the simulations through the transformation coordinate option (TR card) of the MCNPX code. The collimator was made of lead and 549 holes were considered in its model. The simulated fan-beam collimator was of the converging type along the x-axis and of the parallel-hole type along the y-axis. Specifications of the simulated fan-beam collimator are listed in Table 1.

A diagram of the modeled fan-beam collimator along with the simulated gamma camera is shown in Fig. 1.

2.2 Effect of radiation scattering on image quality

To evaluate the effect of scattered radiation on the acquired image quality, the Snyder phantom was simulated with an isotropic ^{99m}Tc point source located inside the phantom. The

Snyder phantom simulates the human head and comprises of three different layers including skin, skull (cranium), and brain, which are described by the following equations [15]:

$$\begin{aligned}
&\left(\frac{x}{7.3}\right)^2+\left(\frac{y}{10.3}\right)^2+\left(\frac{z}{8.8}\right)^2=1 \quad \text{for skin}\\
&\left(\frac{x}{8.6}\right)^2+\left(\frac{y}{9.8}\right)^2+\left(\frac{z}{8.3}\right)^2=1 \quad \text{for skull}\\
&\left(\frac{x}{6}\right)^2+\left(\frac{y}{9}\right)^2+\left(\frac{z}{6.5}\right)^2=1 \quad \text{for brain.}
\end{aligned} \tag{1}$$

A schematic view of the simulated Snyder phantom at different planes is shown in Fig. 2. The composition and density of different phantom layers were taken from the ICRU 46 report [16].

To evaluate the effect of radiation scattering on image quality, two different scenarios were considered. In the first scenario, the response of the simulated imaging system to an isotropic ^{99m}Tc point source, in the absence of the phantom, was obtained by calculating the PSF and MTF at source-to-collimator distances (SCD) of 2, 4, 6, 8, and 10 cm. In the second scenario, the source was located inside the Snyder phantom at the second state and the corresponding response of the imaging system in terms of the PSF and MTF was obtained at the same source-to-collimator distances. The employed simulation setup for data acquisition from the simulated imaging system in the presence and absence of the Snyder phantom is shown in Fig. 3a, b, respectively.

Finally, the contribution of scattered radiation to image quality degradation was evaluated by comparing the system response in the presence and absence of the Snyder phantom in both spatial and frequency domains. The full width at half-maximum (FWHM) and full width at tenth maximum (FWTM) of the obtained trans-axial PSFs at different

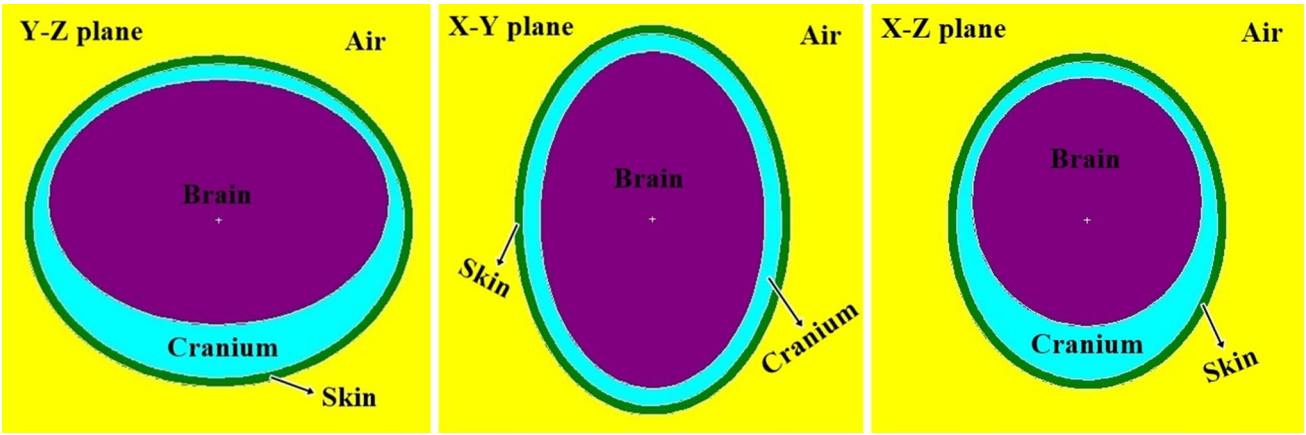

Fig. 2 Schematic diagram of simulated Snyder phantom using MCNPX Monte Carlo code in different planes

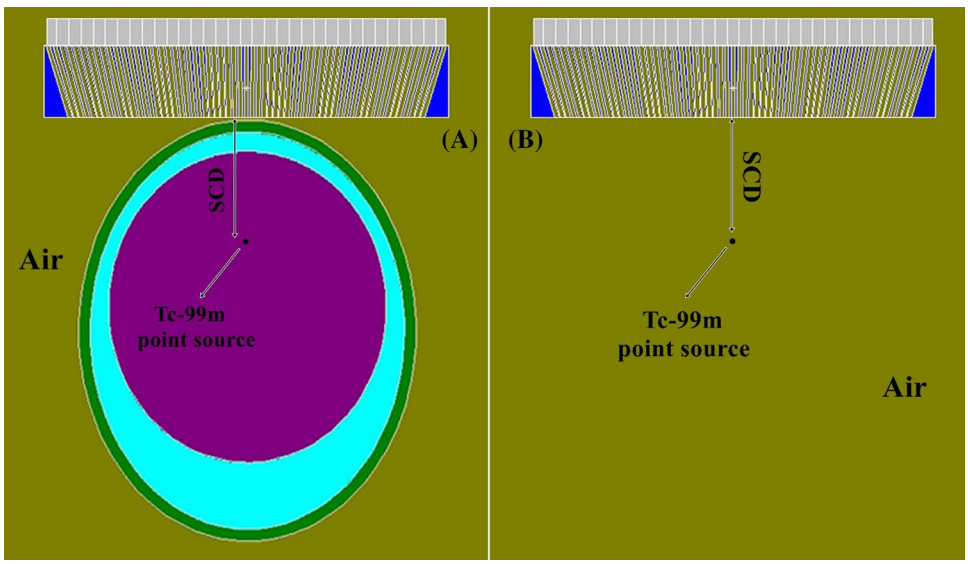

Fig. 3 Simulation setup employed to obtain imaging system response in **a** presence and **b** absence of Snyder phantom. As shown in this figure, the Snyder phantom is substituted by the air in the performed simulations in the absence of scattering media. *SCD* source-to-collimator distance

distances were considered in the spatial domain. Meanwhile, the spatial frequency (in terms of cycles/cm) at nine-tenths ($SF_{0.9}$) and one-tenth ($SF_{0.1}$) of the maximum MTF (= 1) were extracted and compared in the frequency domain. It should be noted that the focal length of the simulated fan-beam collimator was always the same in all of preformed simulations (350 mm) and was not changed when the distance between the radiation source and the fan-beam collimator was increased.

The energy window for data acquisition was tuned to 20% (126–154 keV) in all simulations. A total of 500,000,000 histories were followed in all the preformed simulations and the response of gamma camera was calculated by the F8 tally (the pulse height scoring tally). A standard computing system (CPU Intel Core i7/RAM 8 GB) was used for simulations, so that the time of each simulation was approximately 1200 min. The associated statistical error with the obtained Monte Carlo results was less than 3%.

3 Results

The energy response of the simulated gamma camera to the emitted gamma rays from the ^{99m}Tc source is shown in Fig. 4. It should be noted that the presented data are normalized to the maximum registered counts.

As shown in Fig. 4, the statistical fluctuations in the gamma camera response can be observed in the Monte Carlo-based energy spectrum; these are owing to the targeted spreading of the crystal response in simulations. Furthermore, there is a good agreement between the measured and simulated energy spectra for the gamma camera of this study. This confirms the validity of the considered Gaussian energy broadening response for the gamma camera and the accurate performance of the selected energy window for data acquisition. The observed differences between the simulated and measured data in low-energy (0.08–0.12 MeV) and high-energy (about 0.16–0.18 MeV) regions can be mainly attributed to the fact that the electronic modules of the imaging system (such as the PMT, preamplifier, and amplifier) and their corresponding low-amplitude electrical noise as well as high-amplitude overlapped pulses are not considered in the Monte Carlo simulations.

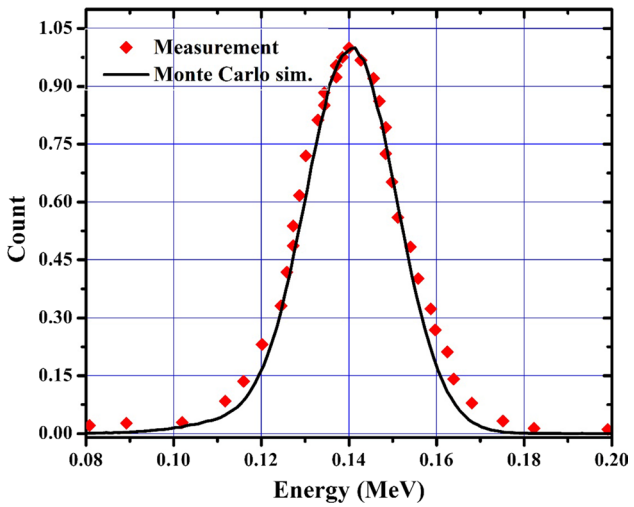

Fig. 4 Comparison of calculated and measured energy response of gamma camera to 140 keV photon energy. Statistical fluctuations in the energy response of the gamma camera are considered during the simulations

The response of the imaging system to a ^{99m}Tc point source in terms of the PSF (in the spatial domain) and the MTF (in the frequency domain) in the absence and presence of the Snyder phantom (scattering media) is shown in Figs. 5 and 6, respectively.

The MTFs were obtained by applying the 2D fast Fourier transform to the PSFs at different distances from the collimator surface. As shown in Figs. 5 and 6, the MTF values at different spatial frequencies in the presence of the phantom are lower than those obtained in the absence of the Snyder phantom. For example, the MTF value at a spatial frequency of 0.3 cycle/cm in the presence of the Snyder phantom decreases by 3.1, 3.9, 4.5, 5.6, and 6.7% at SCDs of 2, 4, 6, 8, and 10 cm, respectively.

The impact of radiation scattering on the image quality in the spatial domain was assessed by a comparison of the FWHM and FWTM of the obtained PSFs at different distances from the collimator in the presence and absence of the Snyder phantom. As recommended by the NEMA Nu-1 protocol [17], the FWHMs and FWTMs of the obtained PSFs at different distances were extracted by the interpolation process.

The comparison between the calculated FWHMs and FWTMs at different distances from collimator surface in the presence and absence of the scattering media (Snyder phantom) is shown in Fig. 7.

An image quality analysis in the frequency domain was performed by comparing the obtained $SF_{0.9}$ and $SF_{0.1}$ values in the presence and absence of the Snyder phantom. The results of this comparison are presented in Fig. 8.

All the obtained results were corrected for magnification by the employed fan-beam collimator at different distances.

4 Discussion

As depicted in Figs. 5 and 6, the width of the obtained PSFs increases with increasing distance from the collimator surface with both the presence and absence of the Snyder phantom. Correspondingly, the cutoff frequency of the obtained MTFs considerably decreases at greater distances from the collimator surface. This result indicates that the distance

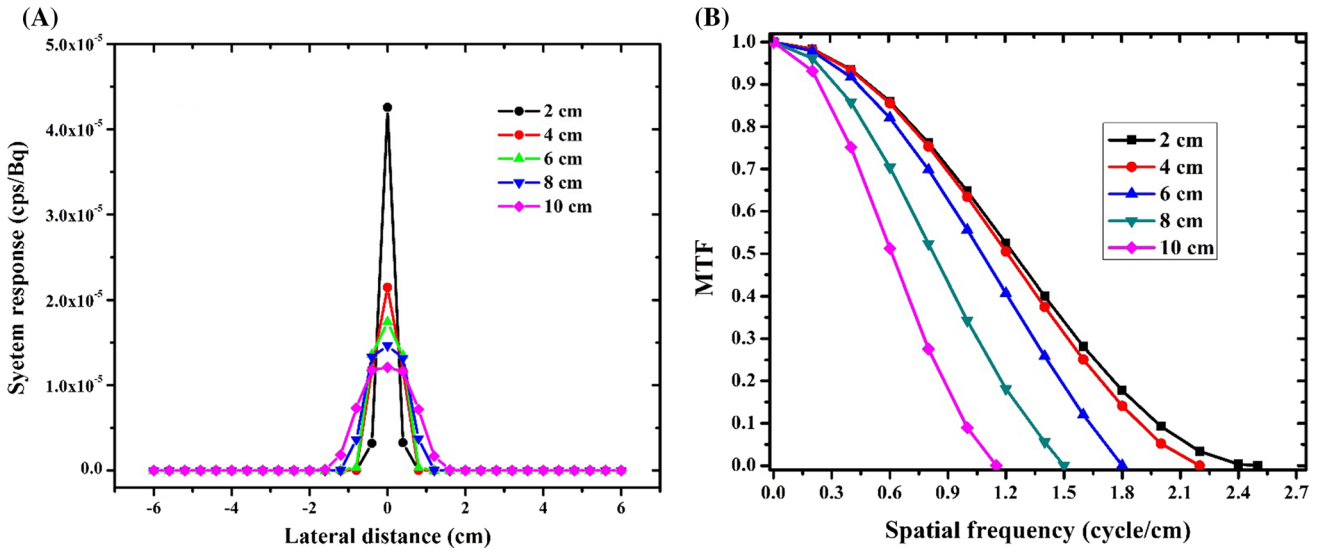

Fig. 5 Response of simulated imaging system [in terms of count per second (cps) per Bq] to an isotropic ^{99m}Tc point source in absence of Snyder phantom (scattering media). **a** Obtained PSFs at different distances from the collimator surface, and **b** depicts the corresponding MTFs which are calculated by the fast Fourier transform (FFT) of obtained PSFs

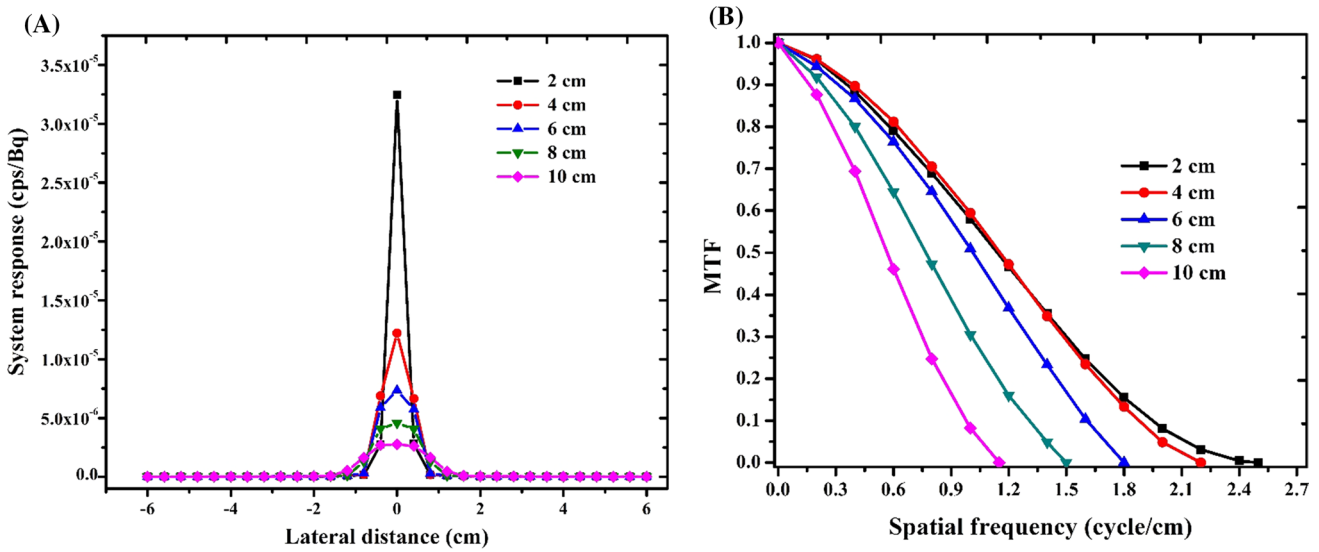

Fig. 6 Response of simulated imaging system [in terms of count per second (cps) per Bq] to an isotropic ^{99m}Tc point source in presence of Snyder phantom (scattering media). **a** Obtained PSFs at different distances from the collimator surface, and **b** depicts the corresponding MTFs, which are calculated by the fast Fourier transform (FFT) of obtained PSFs

between the object and image planes has a remarkable effect on the acquired image quality in terms of spatial and contrast resolution, which deteriorates with increasing distance from the collimator surface.

Variations of the FWHM and FWTM in the presence and absence of scattering media, as shown in Fig. 7, indicate that the scatter radiation originating from the phantom mainly affects the FWTM and has a negligible effect on the FWHM. The maximum difference between the obtained FWTM in the presence and absence of the phantom was 14%, while this difference was approximately 5% for the extracted FWHM from the obtained PSFs. Scattered photons are mainly registered at greater distances from the detector center and consequently affect the FWTM largely. With respect to the fact that the FWHM and FWTM affect the spatial and image contrast resolution, respectively [2], it can be deduced that the photons scattered by the brain tissue will deteriorate the contrast resolution, while they

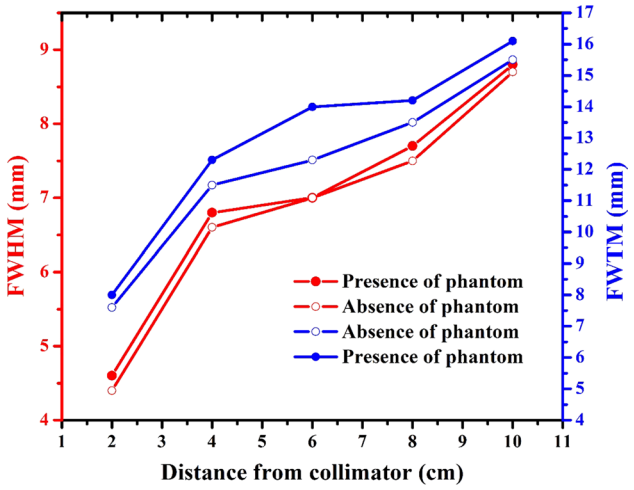

Fig. 7 Extracted FWHM and FWTM from obtained PSFs at different distances from collimator surface in presence and absence of scattering media (Snyder phantom)

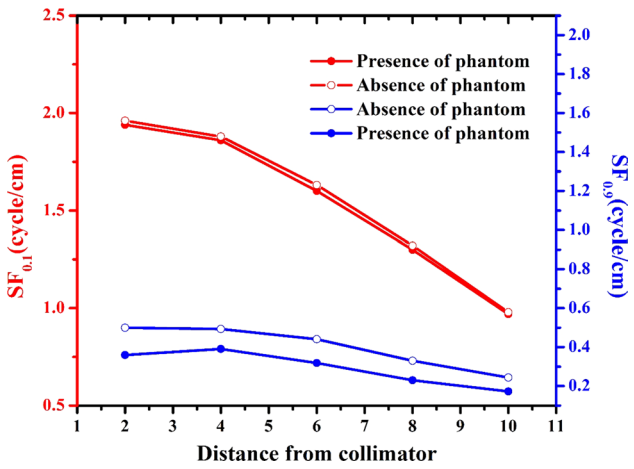

Fig. 8 Calculated spatial frequencies at 10% and 90% of maximum MTF ($SF_{0.1}$ and $SF_{0.9}$, respectively) at different distances from collimator surface in presence and absence of scattering media (Snyder phantom)

do not have a remarkable effect on the spatial resolution of the image.

As shown in Fig. 8, the scattered radiation mainly affects the $SF_{0.9}$ values, while its effect on $SF_{0.1}$ values is negligible. The maximum difference between the obtained $SF_{0.9}$ values in the presence and absence of scattering media was 43%. In contrast, the observed maximum difference for $SF_{0.1}$ in the two cases was a mere 2%.

As the spatial frequency at one-tenth of the maximum MTF ($SF_{0.1}$) is a measure of spatial resolution [18], it can be concluded that radiation scattering does not considerably affect the spatial resolution of the image.

A comparison of the image parameters in both the spatial and the frequency domains reveals that the frequency domain more effectively distinguishes the effects of radiation scattering on image quality. As described above, the maximum difference between the obtained results with and without the phantom in the spatial domain was 14%, while this difference was 43% in the frequency domain. The findings of this study show that the spatial frequency at nine-tenths of the maximum MTF ($SF_{0.9}$) can be considered a good parameter for the quantitative evaluation of the radiation scattering effect on image quality in the frequency domain.

Although a simple single energy window (126–154 keV) was considered for scatter compensation during data acquisition in the current study, more accurate and effective scatter rejection methods such as dual-energy window, dual-photopeak window, and three-energy window [19–21] can be employed to compensate the effects of poor energy resolution of the NaI gamma camera (approximately 10% at a photon energy of 140 keV [22]) and further reduce the contribution of the scattered photons to image quality degradation.

5 Conclusion

In this study, a SPECT imaging system in conjunction with a fan-beam collimator was simulated using the Monte Carlo method. The effects of radiation scattering on brain image quality were determined by a quantitative comparison of the imaging system's response in the presence and absence of scattering media (Snyder phantom). This comparison was performed in both spatial and frequency domains.

The results show that radiation scattered from the patient has a remarkable contribution to image quality degradation in terms of contrast resolution, while it does not have a significant impact on the spatial resolution of the acquired images.

The effects of radiation scattering are more obvious in the frequency domain, and the imaging system response is evaluated in terms of the MTF.

Funding None.

Compliance with ethical standards

Conflict of interest The authors declare that they have no conflict of interests.

Ethical approval This article does not involve any studies with human participants or animals performed by any of the authors.

Informed consent None.

References

1. Prekeges J. Nuclear medicine instrumentation. Burlington: Jones & Bartlett Publishers; 2010.
2. Bushberg JT, Boone JM. The essential physics of medical imaging. Philadelphia: Lippincott Williams & Wilkins; 2012.
3. Van Audenhaege K, Van Holen R, Vandenberghe S, Vanhove C, Metzler SD, Moore SC. Review of SPECT collimator selection, optimization, and fabrication for clinical and preclinical imaging. Med Phys. 2015;42:4796–813.
4. Ter-Antonyan R, Jaszczak RJ, Greer KL, Bowsher JE, Metzler SD, Coleman RE. Combination of converging collimators for high-sensitivity brain SPECT. J Nucl Med. 2009;50:1548–56.
5. Pareto D, Pavía J, Falcón C, Juvells I, Cot A, Ros D. Characterisation of fan-beam collimators. Eur J Nucl Med. 2001;28:144–9.
6. Park MA, Moore SC, Kijewski MF. Brain SPECT with short focal-length cone-beam collimation. Med Phys. 2005;32:2236–44.
7. Capote RM, Matela N, Conceição RC, Almeida P. Optimization of convergent collimators for pixelated SPECT systems. Med Phys. 2013;40:062501.
8. Li T, Wen J, Liang Z. Analytical compensation for spatially variant detector response in SPECT with varying focal-length fan-beam collimators. IEEE Trans Nucl Sci. 2003;50:398–404.
9. Pareto D, Cot A, Pavía J, Falcón C, Juvells I, Lomeña F, et al. Iterative reconstruction with correction of the spatially variant fan-beam collimator response in neurotransmission SPET imaging. Eur J Nucl Med Mol Imaging. 2003;30:1322–9.
10. Pareto D, Cot A, Falcon C, Juvells I, Pavıa J, Ros D. Geometrical response modeling in fan-beam collimators. A numerical simulation. IEEE Trans Nucl Sci. 2002;49:17–24.
11. GE Healthcare Data Sheet Report. Discovery NM/CT 670. https://www.gehealthcare.com/-/media/450f4f8bafbb4bd7a18d37185a0dc073.pdf?la=en&hash=37D82292B3CE4B919CA86687894D24B3199E125B. Accessed 10 June 2018.
12. Pelowitzs DB. MCNPX user's manual, version 2.6.0. Los Alamos: Los Alamos National Laboratory; 2008.
13. Less JE, Fraser GW, Keay A, Bassford D, Ott R, Ryder W. The high resolution gamma camera imager (HRGI): a CCD based camera for medical imaging. Nucl Instr Methods Phys Res. 2003;513:23–6.
14. Boren EL, Delbeke D, Patton JA, Sandler MP. Comparison of FDG PET and positron coincidence detection imaging using a dual-head gamma camera with 5/8-inch NaI(Tl) crystals in patients with suspected body malignancies. Eur J Nucl Med. 1999;26:379–87.
15. Rasouli FS, Masoudi SF. Simulation of the BNCT of brain tumors using MCNP code: beam designing and dose evaluation. Iran J Med Phys. 2012;9:182–92.
16. ICRU 46. Photon, electron, proton and neutron interaction data for body tissues. International Commission on Radiation Units and Measurements, Bethesda; 1992.
17. NEMA, National Electrical Manufacturers Association Standards Publication NU 1-2007: Performance measurements of gamma cameras. Washington DC; 2007.
18. Arabi H, Kamali Asl AR, Ay MR, Zaidi H. Novel detector design for reducing inter-cell X-ray cross-talk in the variable resolution X-ray CT scanner: a Monte Carlo study. Med Phys. 2011;38:1389–96.
19. Jaszczak RJ, Greer KL, Floyd CE Jr, Harris CC, Coleman RE. Improved SPECT quantification using compensation for scattered photons. J Nucl Med. 1984;25:893–900.
20. King MA, Hademenos GJ, Glick SJ. A dual-photopeak window method for scatter correction. J Nucl Med. 1992;33:605–12.
21. Ogawa K, Harata Y, Ichihara T, Kubo A, Hashimoto S. A practical method for position dependent Compton-scatter correction in single photon emission CT. IEEE Trans Med Imaging. 1991;10:408–12.
22. Noori Asl M, Sadremomtaz AR, Bitarafan-Rajabi A. Evaluation of six scatter correction methods based on spectral analysis in 99mTc SPECT imaging using SIMIND Monte Carlo simulation. J Med Phys. 2013;38:189–97.